SENSITIVITY OF SEISMIC WAVES TO THE STRUCTURE

AUTHOR
L. KLIMEŠ
Address
Department of Geophysics, Charles University, Ke Karlovu 3, 121 16 Praha 2, Czech Republic
E-mail: klimes@sw3d.mff.cuni.cz

Summary

We study how the perturbations of a generally heterogeneous isotropic or anisotropic structure manifest themselves in the wavefield, and which perturbations can be detected within a limited aperture and a limited frequency band. A broad–band incident wavefield with a smooth frequency spectrum is considered. Infinitesimally small perturbations of elastic moduli and density are decomposed into Gabor functions. The wavefield scattered by the perturbations is then composed of waves scattered by individual Gabor functions. The scattered waves are estimated using the first–order Born approximation with paraxial ray approximation.

Each Gabor function generates at most 5 scattered waves, propagating in specific directions. A Gabor function corresponding to a low wavenumber may generate a single broad–band unconverted wave scattered in forward or narrow–angle directions. A Gabor function corresponding to a high wavenumber usually generates 0 to 5 narrow–band Gaussian packets scattered in wide angles, but may also occasionally generate a narrow–band P to S converted Gaussian packet scattered in a forward direction, or a broad–band S to P converted wave scattered in wide angles.

For a particular source, each wave scattered by a Gabor function at a given spatial location is sensitive to just a single linear combination of 22 values of the elastic moduli and density corresponding to the Gabor function. This information about the Gabor function is lost if the scattered wave does not fall into the aperture covered by the receivers and into the legible frequency band.

1. Gabor representation of medium perturbations

We consider infinitesimally small perturbations $\delta c_{ijkl}(\mathbf{x})$ and $\delta\varrho(\mathbf{x})$ of elastic moduli $c_{ijkl}(\mathbf{x})$ and density $\varrho(\mathbf{x})$ in elastodynamic equation

$$\varrho(\mathbf{x})\ \ddot{u}_i(\mathbf{x},t) = [c_{ijkl}(\mathbf{x})\ u_{k,l}(\mathbf{x},t)]_{,j} + f_i(\mathbf{x},t) \quad .$$

The perturbations are decomposed into Gabor functions $g^\alpha(\mathbf{x})$,

$$\delta c_{ijkl}(\mathbf{x}) = \sum_\alpha c^\alpha_{ijkl}\ g^\alpha(\mathbf{x}) \quad , \qquad \delta\varrho(\mathbf{x}) = \sum_\alpha \varrho^\alpha g^\alpha(\mathbf{x}) \quad ,$$

where the Gabor functions

$$g^\alpha(\mathbf{x}) = \exp[\mathrm{i}\mathbf{k}^{\alpha\,\mathrm{T}}(\mathbf{x}-\mathbf{x}^\alpha) - \tfrac{1}{2}(\mathbf{x}-\mathbf{x}^\alpha)^{\mathrm{T}}\mathbf{K}^\alpha(\mathbf{x}-\mathbf{x}^\alpha)]$$

are centred at various spatial positions $\mathbf{x}^\alpha$ and have various structural wavenumber vectors $\mathbf{k}^\alpha$. The wavefield scattered by the perturbations is then composed of waves $u^\alpha_i(\mathbf{x},t)$ scattered by individual Gabor functions,

$$\delta u_i(\mathbf{x},t) = \sum_\alpha u^\alpha_i(\mathbf{x},t) \quad ,$$

see Figures 1, 2, 3.

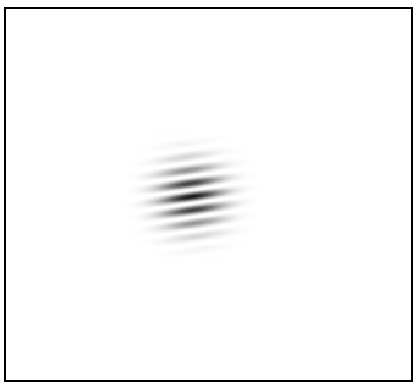

Figure 1. A single Gabor function $g^\alpha(\mathbf{x})$ at point $\mathbf{x}^\alpha$.

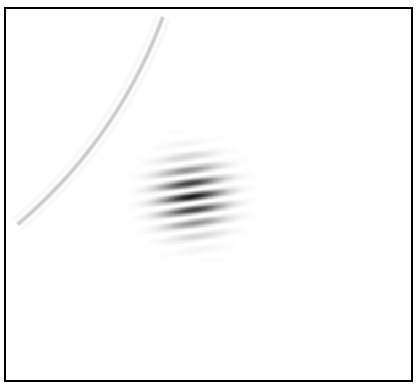

Figure 2. Broad–band wave $u_i(\mathbf{x},t)$ incident at the Gabor function.

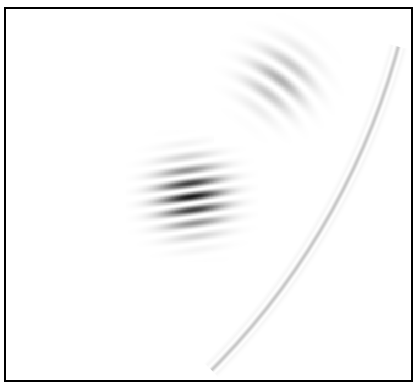

Figure 3. Scattered wave $u^\alpha_i(\mathbf{x},t)$.

2. Applied approximations

The first–order sensitivity of the wavefield to the infinitesimally small structural perturbations is exactly described by the *first–order Born approximation*

$$u^\alpha_i(\mathbf{x},t) = -\int\mathrm{d}\mathbf{x}'\int\mathrm{d}t' g^\alpha(\mathbf{x}')\big[\dot{G}_{im}(\mathbf{x},\mathbf{x}',t-t')\ \varrho^\alpha\ \dot{u}_m(\mathbf{x}',t') + G_{im,j}(\mathbf{x},\mathbf{x}',t-t')\ c^\alpha_{mjkl}\,u_{k,l}(\mathbf{x}',t')\big] \quad ,$$

where the spatial partial derivatives are related to coordinates x'_i. The Green tensor is defined by equation

$$\varrho(\mathbf{x})\ \ddot{G}_{im}(\mathbf{x},\mathbf{x}',t) = [c_{ijkl}(\mathbf{x})\ G_{km,l}(\mathbf{x},\mathbf{x}',t)]_{,j} + \delta_{im}\,\delta(\mathbf{x}-\mathbf{x}')\,\delta(t) \quad ,$$

where the spatial partial derivatives are related to coordinates x_i.

The *paraxial ray approximation* of both incident wave $u_k(\mathbf{x}', t')$ and Green tensor $G_{im,j}(\mathbf{x}, \mathbf{x}', t)$ is applied in the vicinity of point $\mathbf{x}^\alpha$. The paraxial ray approximation consists in a constant amplitude and in the second–order Taylor expansion of travel time at point $\mathbf{x}^\alpha$.

We use the *high–frequency approximation of spatial derivatives*,

$$u_{i,k}(\mathbf{x}', t) \approx -\dot{u}_i(\mathbf{x}', t)\ P_k(\mathbf{x}^\alpha) \quad , \qquad \frac{\partial G_{ij}}{\partial x'_k}(\mathbf{x}, \mathbf{x}', t) \approx \dot{G}_{ij}(\mathbf{x}, \mathbf{x}', t)\ p_k(\mathbf{x}^\alpha) \quad ,$$

where $P_i(\mathbf{x}) = \tau_{,i}(\mathbf{x})$ is the slowness vector of the incident wave, and $p_k(\mathbf{x}^\alpha)$ is the slowness vector determining the ray leading from point $\mathbf{x}^\alpha$ to the receiver.

3. Scattering in the frequency domain — Gaussian beams

A *broad–band incident wavefield* having a smooth frequency spectrum is considered, with a frequency band limited by the minimum frequency and the maximum frequency. The Fourier transform of the incident wave in the vicinity of point $\mathbf{x}^\alpha$ is assumed in form

$$\widehat{u}_i(\mathbf{x}, \omega) = \widehat{A}(\omega) E_i \exp[\mathrm{i}\omega\tau(\mathbf{x})]$$

with amplitude $\widehat{A}(\omega)$, polarization E_i and travel time τ. For each frequency ω, the scattered wavefield consists of at most one P–wave Gaussian beam or of at most two S–wave Gaussian beams. A Gaussian beam is generated if structural wavenumber vector k^α is close to the corresponding *"wavenumber surface"* $\mathcal{S}_{\mathbf{P}\omega}$, defined by transformation

$$\mathbf{p} \in \mathcal{S} \longrightarrow \mathbf{k} = (\mathbf{p} - \mathbf{P})\,\omega \in \mathcal{S}_{\mathbf{P}\omega}$$

of the slowness surface $\mathcal{S}$. The transformation is illustrated in Figures 4, 5, 6.

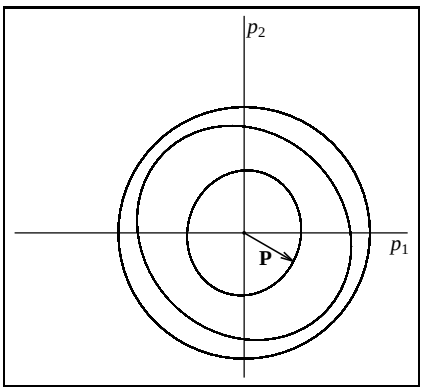

Figure 4. Slowness surface $\mathcal{S}$.

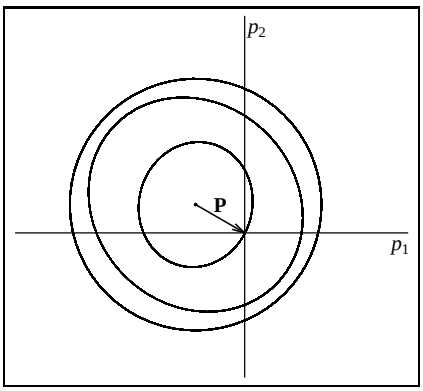

Figure 5. Shifted slowness surface $\mathcal{S}_{\mathbf{P}}$.

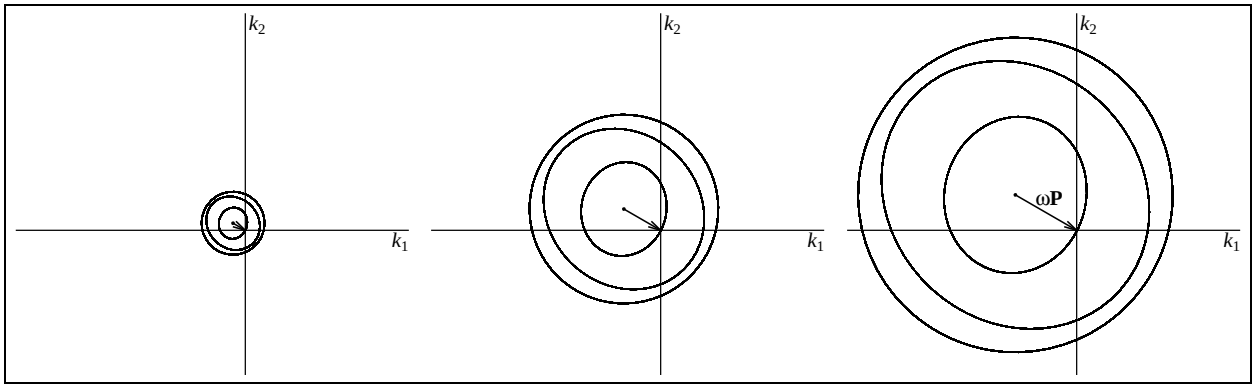

Figure 6. Wavenumber surfaces $\mathcal{S}_{\mathbf{P}\omega}$ at various positive frequencies ω.

The amplitude of the *Gaussian beam* scattered by Gabor function $g^\alpha(\mathbf{x})$ at positive frequency ω is

$$\widehat{a}(\omega) = \mathrm{i}\omega\widehat{A}(\omega)\sqrt{2\pi\, m^{-1}}\ r\ \exp(-\tfrac{1}{2}\|\Delta\mathbf{k}\|^2) \ ,$$

where

$$r = \frac{\varrho^\alpha E_m e_m - c^\alpha_{ijkl} E_i P_j e_k p_l}{2\ \varrho} \qquad (\bullet)$$

is the "reflectivity function". Here P_i and E_i are the slowness vector and the polarization vector of the incident wave, p_i and e_i are the slowness vector and the polarization vector of the scattered wave at point $\mathbf{x}^\alpha$. Density ϱ corresponds to the background.

$\|\Delta\mathbf{k}\|$ is the distance from the wavenumber surface $\mathcal{S}_{\mathbf{P}\omega}$. The distance is defined in terms of the "wavenumber metric tensor",

$$\|\Delta\mathbf{k}\|^2 = \Delta\mathbf{k}^{\mathrm{T}}[\mathbf{K}^\alpha + \omega^2\mathbf{T}(\mathbf{K}^\alpha)^{-1}\mathbf{T}]^{-1}\Delta\mathbf{k} \quad ,$$

where

$$T_{ij} = \frac{\partial^2\tau}{\partial x_i \partial x_j} + \frac{H_{,i}p_j + p_i H_{,j}}{H^{,k}p_k} - \frac{p_i p_j H^{,m} H_{,m}}{(H^{,k}p_k)^2} \quad .$$

Here

$$H_{,i} = \frac{\partial H}{\partial x_i} \quad , \qquad H^{,i} = \frac{\partial H}{\partial p_i}$$

are the derivatives of Hamiltonian $H = H(x_m, p_n)$ corresponding to the Gaussian beam scattered at point $\mathbf{x}^\alpha$. Exponential weighting $\exp(-\frac{1}{2}\|\Delta\mathbf{k}\|^2)$ is illustrated in Figure 7.

The square root $\sqrt{2\pi m^{-1}}$, where

$$m = H^{,i}(K_{ij} - \mathrm{i}\omega T_{ij})H^{,j}\ (H^{,k}p_k)^{-2} \quad ,$$

represents the integral of function

$$\exp[-\tfrac{1}{2}(\mathbf{x}-\mathbf{x}^\alpha)^{\mathrm{T}}(\mathbf{K}^\alpha-\mathrm{i}\omega\mathbf{T})(\mathbf{x}-\mathbf{x}^\alpha)]$$

with respect to travel time along the central ray of the scattered Gaussian beam.

The initial shape of a Gaussian beam is determined by the projection of matrix $(\mathbf{K}^\alpha-\mathrm{i}\omega\mathbf{T})^{-1}$ onto the plane perpendicular to the central ray of the beam.

A scattered Gaussian beam has a maximum amplitude if $\|\Delta\mathbf{k}\|=0$, i.e., if $\mathbf{k}^\alpha\in\mathcal{S}_{\mathbf{P}\omega}$. For each $\mathbf{k}^\alpha$, there are at most 5 finite positive frequencies $\omega=\omega_0$ such that $\mathbf{k}^\alpha\in\mathcal{S}_{\mathbf{P}\omega_0}$. The frequencies ω_0 are solutions of the sixth–order equation

$$\det[c_{ijkl}(P_i+\omega_0^{-1}k_i)(P_l+\omega_0^{-1}k_l)-\varrho\delta_{jk}]=0$$

for the eigenvalues of the Christoffel matrix (the equation has one infinite trivial solution $\omega_0=+\infty$).

For $\mathbf{k}^\alpha\in\mathcal{S}_{\mathbf{P}\omega_0}$, the central ray of the scattered Gaussian beam pass through point $\mathbf{x}^\alpha$, and its initial slowness vector is

$$\mathbf{p}_0=\mathbf{P}+\omega_0^{-1}\mathbf{k}^\alpha\quad .$$

For $\mathbf{k}^\alpha$ from the vicinity of wavenumber surface $\mathcal{S}_{\mathbf{P}\omega_0}$, the initial point and initial slowness vector of the central ray of the scattered Gaussian beam slightly depend on frequency, scattering different frequencies to different directions.

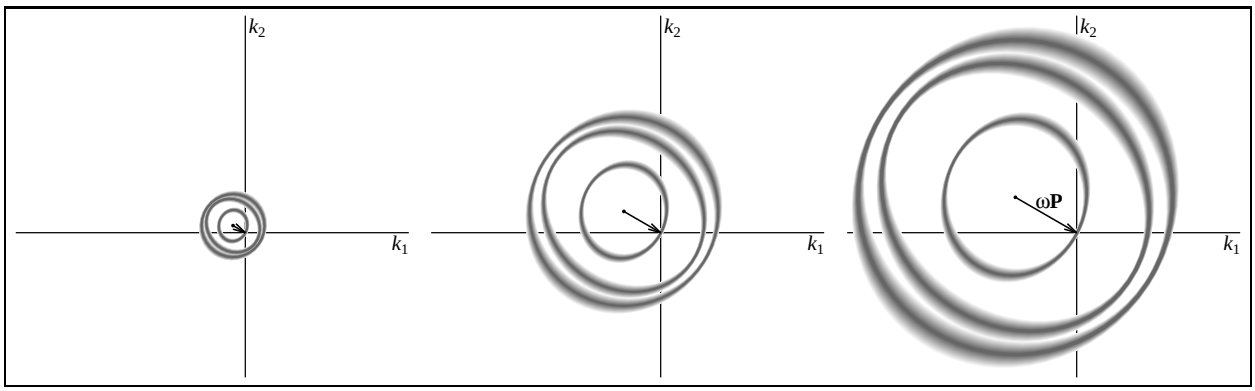

Figure 7. Sensitivity of scattered Gaussian beams to structural wavenumbers at various positive frequencies ω, given by weighting factor $\exp(-\frac{1}{2}\|\Delta\mathbf{k}\|^2)$.

4. Scattering in the time domain — Gaussian packets

Scattered waves in the time domain can be composed of the scattered frequency–domain Gaussian beams.

4.1 Narrow–band scattering

There are at most 5 finite positive frequencies $\omega=\omega_0$ such that $\mathbf{k}^\alpha\in\mathcal{S}_{\mathbf{P}\omega_0}$. If $\mathbf{k}^\alpha$ is sufficiently deviated from the tangent plane to $\mathcal{S}_{\mathbf{P}\omega_0}$ at $\mathbf{k}^\alpha$, the beams are scattered in a narrow Gaussian frequency band centred at ω_0, forming a space–time Gaussian wave packet of prevailing frequency ω_0.

We shall refer to the set of wavenumber vectors $\mathbf{k}^\alpha$, causing narrow–band scattering, as the "high–wavenumber domain", see Figure 8. For each particular incident wave, the broad–band wavefield, scattered by a Gabor function belonging to this domain, consists of at most 5 narrow–band space–time Gaussian wave packets. Each recorded Gaussian packet is localized in the time section (set of seismograms corresponding to the source).

This is typical wide–angle scattering, but occurs also for P to S forward and narrow–angle scattering. The high–wavenumber domain is usually being recovered by seismic migration or by diffraction tomography.

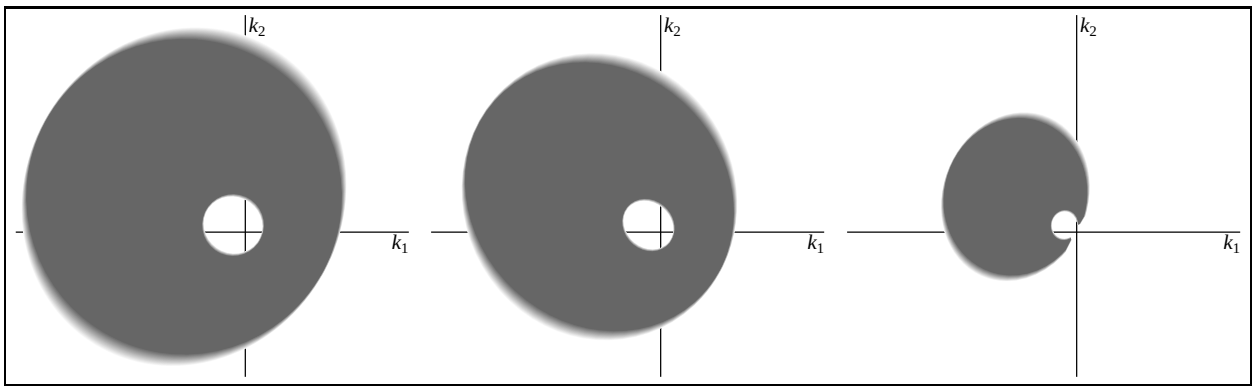

Figure 8. High–wavenumber domain, consisting of the structural wavenumbers generating narrow–band Gaussian packets. Three charts correspond to three polarizations of the scattered wave. Note that different polarizations and different directions of the structural wavenumber vector $\mathbf{k}^\alpha$ are sensitive to different linear combinations (•) of perturbations of elastic moduli and density. When changing the source, the wavenumber domain of sensitivity "rotates" with the direction of the incident wavefield, and the reflectivity function (•) changes, allowing to resolve more elastic moduli.

4.2 Broad–band scattering

If the deviation of $\mathbf{k}^\alpha$ from the tangent plane to $\mathcal{S}_{\mathbf{P}\omega_0}$ at $\mathbf{k}^\alpha$ is small, or if $\mathbf{k}^\alpha$ is small, the beams are scattered in a broad frequency band. In this case, the time dependence of the incident wavefield can be decomposed into narrow-band Gabor signals using the Gabor transform. The scattered beams of each narrow–band component of the broad–band incident wavefield form a single space–time Gaussian packet. Gaussian packets of different prevailing

frequencies propagate in different directions, forming a broad–band fan of narrow–band Gaussian packets. The existence and scattering angle of a Gaussian packet depends on the structural wavenumber vector $\mathbf{k}^\alpha$.

This is typical forward and narrow–angle scattering at low wavenumbers $\|\mathbf{k}^\alpha\|$, but occurs also for S to P wave scattering at high wavenumbers $\|\mathbf{k}^\alpha\|$. For a particular incident wave, there may be 2 different kinds of broad–band fans of scattered narrow–band Gaussian packets: one belonging to low wavenumbers $\|\mathbf{k}^\alpha\|$ ($\omega^0 = +\infty$), the other belonging to $\mathbf{k}^\alpha$ from the conical surface tangent to the P–wave sheets of the wavenumber surfaces $\mathcal{S}_{\mathbf{P}\omega}$ during S to P wave scattering (finite ω^0).

We shall refer to the set of low wavenumber vectors $\mathbf{k}^\alpha$, causing forward or narrow–angle broad–band scattering without wave conversion, as the "low–wavenumber domain", see Figure 9. The scattering angle of the Gaussian packet, generated by a Gabor function belonging to the low–wavenumber domain, is inversely proportional to the prevailing frequency of the packet. The low–wavenumber domain is usually being recovered by travel–time tomography and wave–equation tomography.

Note that the union of low–wavenumber domains corresponding to different incident waves may overlap with the union of high–wavenumber domains corresponding to different incident waves.

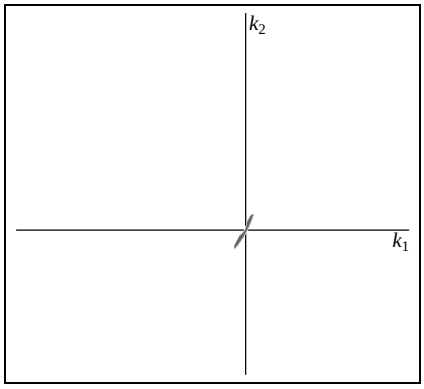

Figure 9. Low–wavenumber domain, consisting of the structural wavenumbers generating a broad–band scattered wavefield.

5. Limited aperture

In geophysics, the aperture covered by the receivers is usually limited (e.g., to an area on the Earth surface). Then only a fraction of scattered time–harmonic Gaussian beams is registered (compare Figures 7 and 10). Consequently, only the time–domain waves scattered by Gabor functions corresponding to the wavenumber vectors from the cones covered by the aperture are registered (compare Figures 8 and 11). The lost information on the on the corresponding linear combination ($\bullet$) of elastic moduli usually cannot be recovered without additional a priori assumptions.

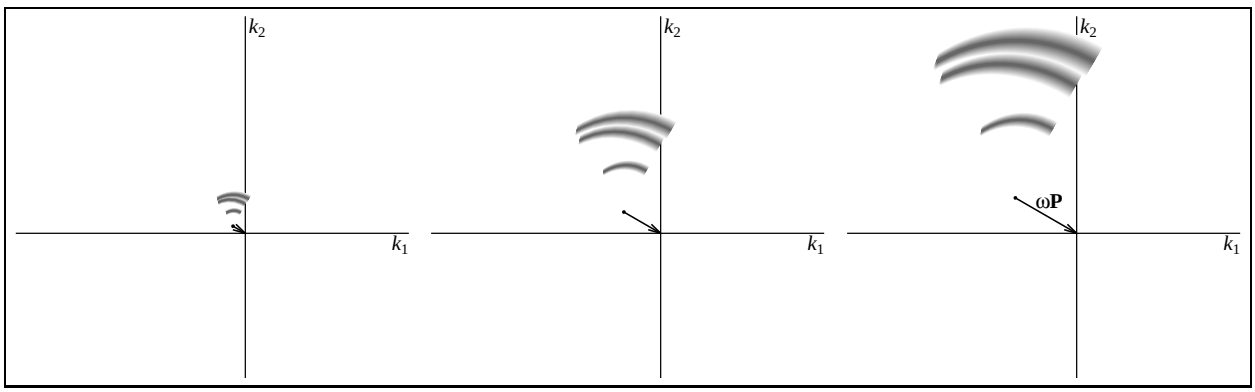

Figure 10. Scattering in the frequency domain — sensitivity of scattered Gaussian beams to structural wavenumbers at various positive frequencies ω for limited aperture.

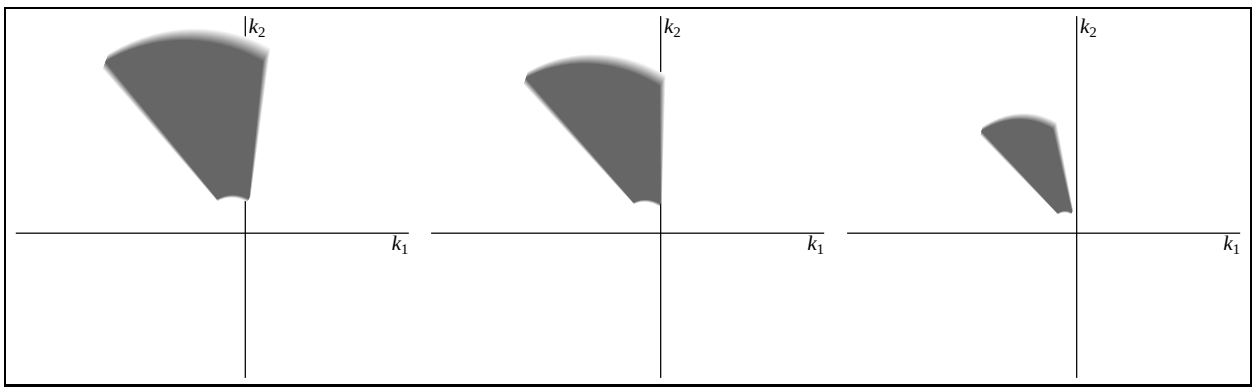

Figure 11. Scattering in the time domain — wavenumbers affecting the wavefield scattered within a limited aperture.

6. Final remark

The derived correspondence between the perturbations of the structure and the recorded wavefield may play a decisive role in understanding the information on geological structures carried by seismic wavefields, in understanding the physical meaning of velocity macro models, and in interpretation of seismic data from forward to wide–angle scattering. It may allow us to understand the physical meaning and resolution of migrated images, and to estimate mispositioning and fuzziness of structural details due to inaccuracies in the velocity macro model.

Acknowledgements

The research has been supported by the Grant Agency of the Czech Republic under Contracts 205/01/0927 and 205/01/D097, by the Grant Agency of the Charles University under Contracts 237/2001/B-GEO/MFF and 229/2002/B-GEO/MFF, by the Ministry of Education of the Czech Republic within Research Project MSM113200004, and by the members of the consortium "Seismic Waves in Complex 3-D Structures" (see "http://sw3d.mff.cuni.cz").